

# Estimation and propagation of volcanic source parameter uncertainty in an ash transport and dispersal model: application to the Eyjafjallajökull plume of 14–16 April 2010

Marcus Bursik · Matthew Jones · Simon Carn ·  
Ken Dean · Abani Patra · Michael Pavolonis ·  
E. Bruce Pitman · Tarunraj Singh · Puneet Singla ·  
Peter Webley · Halldor Bjornsson · Maurizio Ripepe

Received: 24 April 2012 / Accepted: 23 September 2012  
© Springer-Verlag Berlin Heidelberg 2012

**Abstract** Data on source conditions for the 14 April 2010 paroxysmal phase of the Eyjafjallajökull eruption, Iceland, have been used as inputs to a trajectory-based eruption column model, bent. This model has in turn been adapted to generate output suitable as input to the volcanic ash transport and dispersal model, puff, which was used to propagate the paroxysmal ash cloud toward and over Europe over the following days. Some of the source parameters, specifically vent radius, vent source velocity, mean grain size of ejecta, and standard deviation of ejecta grain size have been assigned probability distributions based on our lack of knowledge of exact conditions at the source.

These probability distributions for the input variables have been sampled in a Monte Carlo fashion using a technique that yields what we herein call the polynomial chaos quadrature weighted estimate (PCQWE) of output parameters from the ash transport and dispersal model. The advantage of PCQWE over Monte Carlo is that since it intelligently samples the input parameter space, fewer model runs are needed to yield estimates of moments and probabilities for the output variables. At each of these sample points for the input variables, a model run is performed. Output moments and probabilities are then computed by properly summing the weighted values of the output parameters of interest. Use

---

Editorial responsibility: M. Manga

**Electronic supplementary material** The online version of this article (doi:10.1007/s00445-012-0665-2) contains supplementary material, which is available to authorized users.

---

M. Bursik (✉)  
Department of Geology, University at Buffalo,  
Buffalo, NY, USA  
e-mail: mib@buffalo.edu

M. Jones  
Center for Computational Research, University at Buffalo,  
Buffalo, NY, USA

S. Carn  
Geological and Mining Engineering and Sciences,  
Michigan Technological University,  
Houghton, MI, USA

K. Dean · P. Webley  
Geophysical Institute, University of Alaska,  
Fairbanks, AK, USA

A. Patra · T. Singh · P. Singla  
Department of Mechanical and Aerospace Engineering,  
University at Buffalo,  
Buffalo, NY, USA

M. Pavolonis  
NOAA-NESDIS Center for Satellite Applications and Research,  
Camp Springs, MD, USA

E. B. Pitman  
Department of Mathematics, University at Buffalo,  
Buffalo, NY, USA

H. Bjornsson  
Icelandic Meteorological Office,  
Reykjavik, Iceland

M. Ripepe  
Dipartimento di Scienze della Terra,  
Universita degli Studi di Firenze,  
Florence, Italy

of a computational eruption column model coupled with known weather conditions as given by radiosonde data gathered near the vent allows us to estimate that initial mass eruption rate on 14 April 2010 may have been as high as  $10^8$  kg/s and was almost certainly above  $10^7$  kg/s. This estimate is consistent with the probabilistic envelope computed by PCQWE for the downwind plume. The results furthermore show that statistical moments and probabilities can be computed in a reasonable time by using  $9^4=6,561$  PCQWE model runs as opposed to millions of model runs that might be required by standard Monte Carlo techniques. The output mean ash cloud height plus three standard deviations—encompassing c. 99.7 % of the probability mass—compares well with four-dimensional ash cloud position as retrieved from Meteosat-9 SEVIRI data for 16 April 2010 as the ash cloud drifted over north-central Europe. Finally, the ability to compute statistical moments and probabilities may allow for the better separation of science and decision-making, by making it possible for scientists to better focus on error reduction and decision makers to focus on “drawing the line” for risk assessment.

**Keywords** Iceland · Eyjafjallajökull · Plume · Eruption source parameter · Ash transport · Ash dispersal · Uncertainty · Probabilistic hazard map · Aviation safety

## Introduction

The 2010 eruption of Eyjafjallajökull, Iceland, caused havoc for European aviation with ash emissions from 14 April 2010 into May, and one period of peak emissions during 14–18 April (Petersen 2010). To make predictions of the likely position of the ash cloud and issue advisories to the airline industry, the London Volcanic Ash Advisory Center (VAAC) used the NAME computational model (Ryall and Maryon 1998) to calculate long-range, atmospheric ash advection and dispersion. Other VAACs use different but similar computational models (Folch 2012). Such models require input data on volcanic source conditions, particularly eruption plume position, height and width as a function of time, and the distribution of ash within this virtual volcanic cloud. All such models allow ash to settle as single particles (i.e., “dry deposition”), and are therefore able to track (decreasing) ash content. A few models furthermore have an algorithm for microphysics, which allows the estimation of hydrometeor content, sometimes therefore taking into account aggregation and the formation of accretionary lapilli (i.e., “wet deposition”, implemented in FALL3D and ATHAM (Folch 2012; Textor et al. 2006)). The inputs to these models are rarely well-constrained, hence estimates of the uncertainty in the inputs is valuable in making probabilistic predictions of ash cloud motion. The models also

depend on datasets such as the windfield, which have stochastic variability that must be considered. Despite the potential risk to property and life from ash clouds, models that take into consideration the uncertainty and variability in input parameters and datasets using rigorous stochastic methods (Bonadonna et al. 2010; Folch 2012) to produce forecasts with specified uncertainty do not exist. We begin the process of rigorous uncertainty estimation by addressing the problem of propagation of uncertainties in the volcanic input parameters to produce a coherent probabilistic forecast of ash cloud position.

Computational models of volcanic ash cloud transport and dispersion (VATD models), such as NAME and the puff model used here, require as input the mass of ash together with the pyroclast grain size distribution as a function of height and time. Windfield data are also needed. Visual or radar observations of plume height are often used to estimate a mass eruption rate (MER) based on a (poorly constrained) empirical relationship (Sparks et al. 1997). Integrating the MER estimates over the duration of the eruption yields an ash mass that is then propagated by the VATD simulation within a numerical weather prediction (NWP) windfield model. Grain size is more difficult to estimate than is plume height, so a common method of estimation of initial grain size distribution is to assume that all eruptions of a certain type—as determined by plume height or magma type—have somewhat similar grain-size distributions, and therefore grain size measurements for eruption deposits where data are available can be propagated to other eruptions. The problem with using plume height to estimate MER is that there is considerable scatter in the basic empirical relationships (Mastin et al. 2009), and plume height is also strongly dependent on windspeed and other atmospheric conditions (Bursik 2001; Tupper et al. 2009). Thus estimates of ash size and mass that must be used in the VATD model for near real-time forecasting have unknown accuracy and (probably large) error. A further drawback in propagating grain size data from one eruption to another is that the grain size distribution that is injected into the upper plume is strongly dependent on vent characteristics and the amount of water, and resulting ash aggregation, both within the vent and in the atmosphere near the vent. On top of this, small errors in estimates of mass and grain size can cause significant error in subsequent ash motion.

In this contribution, we consider volcanic input uncertainty estimation, by using a physical model of a volcanic eruption column, bent, to generate an input space for the puff VATD model. Using source quantities such as vent size and vent exit velocity, bent provides eruption column outputs such as ash mass or loading, position of ash in the plume, and grain size distribution. In turn these outputs are used as inputs to puff. By using an eruption column model based on fundamental physics rather than a simplified

scaling relationship that excludes important variables or an eruption-to-eruption comparison, a variety of inputs and observations from the volcanic source region, together with their variability, can be modeled and propagated through the now coupled bent and puff models.

In the subsequent sections we characterize and estimate the several volcanic inputs to the computer models. Then, we introduce a probabilistic computational methodology, the polynomial chaos quadrature weighted estimate (PCQWE), to forecast ash cloud movement. PCQWE treats model input parameters as random variables, which are approximated by a polynomial expansion designed to minimize moment errors (Xiu and Karniadakis 2002). This approach provides a quantitative basis for forecasting, together with a robust estimate of the uncertainty in the resulting measures.

## Model inputs

### Characteristics of the eruption column

The summit eruption of Eyjafjallajökull began on 14 April 2010 sometime between about midnight and sunrise, when an eruption column was first noted (Thorkelsson 2012). This strong or paroxysmal phase continued until 18 April. Observations made over these first few days suggest that variable discharge conditions and partial column collapse were major eruption characteristics (Fig. 1). This resulted in the dispersal of low-level, tropospheric ash far downwind. Near-vent observations indicate that eruptive pulses were often characterized by ejection of an initial gas-rich cap from the volcanic vent, followed by a more densely laden

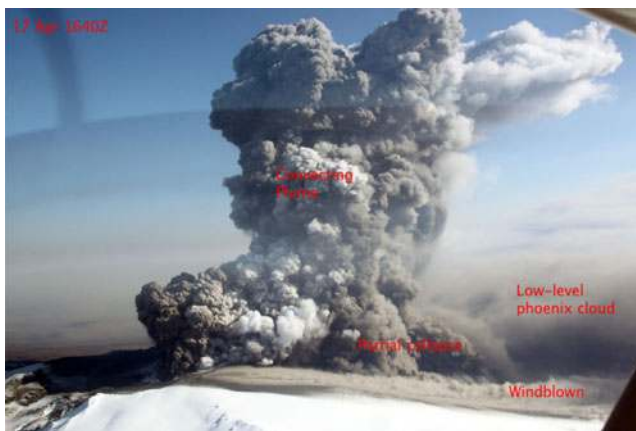


**Fig. 1** Photograph with view to SE of the summit region of Eyjafjallajökull during the initial vigorous eruption phase of 14–18 April. White eddies are water rich, gray are pyroclast rich. The ash blown at low level from the vent produced a voluminous, ground-hugging ash cloud to the south. Photo: M. Roberts, Icelandic Meteorological Office (IMO)

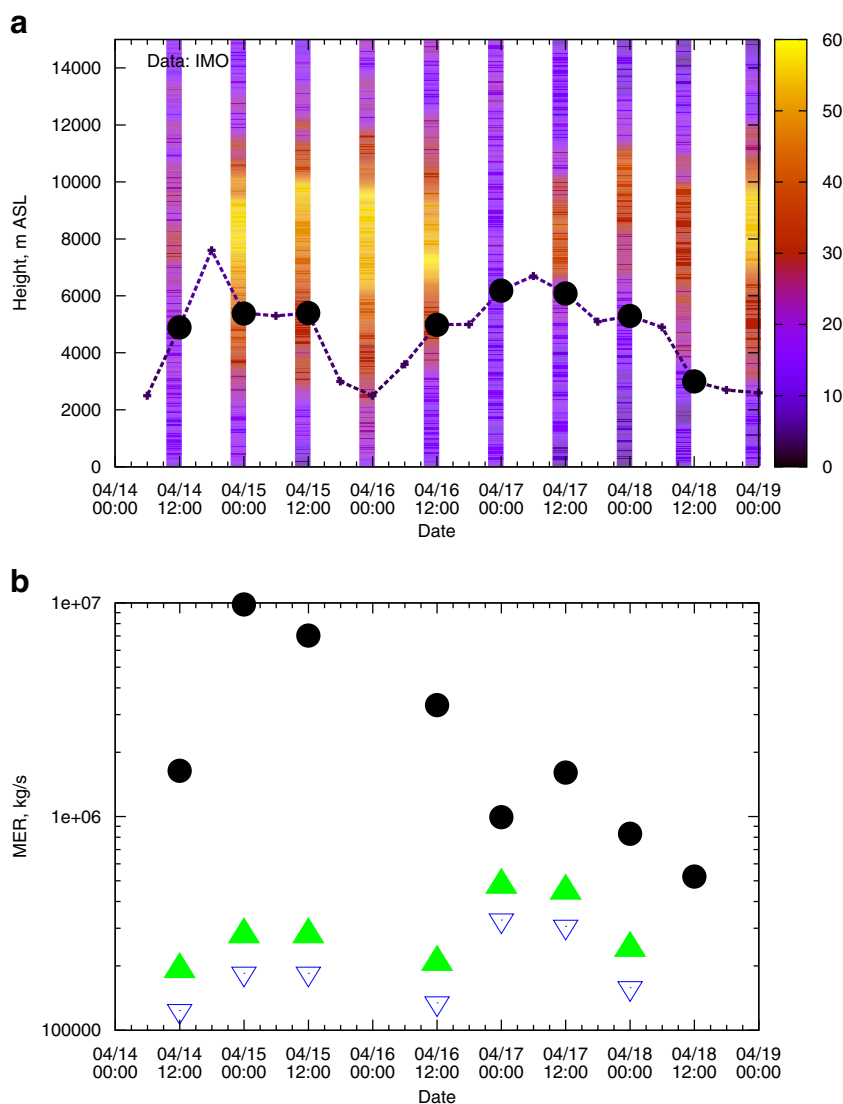
steady flow. There appeared to be no flow separation over the volcano, hence ground-hugging clouds were generally formed by partial column collapse. The result in the proximal region was a higher-level, bent-over column that was often underlain by initially slow-moving, dense eddies coalescing downwind into a lower-level gravity current (phoenix cloud) with a virtual source south of the vent and a sharp upwind edge. Thus, observations of plume rise are consistent with rise height modulated by wind as well as column collapse over the first 5 days of the eruption.

### Model initialization

Ash loading, eruption column height, grain size, and wind-field are thought to be the most important input variables for volcanic ash transport and dispersion modeling (Mastin et al. 2009). The current procedure is to derive mass loading from the product of eruption duration and mass eruption rate (equivalent to mass flux,  $Q$ ). MER in turn is typically calculated from an empirical relationship derived for strong plumes ( $w \gg v$ ), e.g.,  $H_T = 1.67Q^{0.259}$  (Morton et al. 1956; Sparks et al. 1997), where  $w$  is characteristic plume speed (meters per second),  $v$  is wind speed,  $H_T$  is eruption plume height (kilometers), and  $Q$  is mass eruption rate given as the equivalent volume eruption rate (cubic meters per second) assuming a magmatic density ( $3,000 \text{ kg/m}^3$  for basalt in the case of Eyjafjallajökull). This yields ash loading as a function of  $H_T$ . Plume height, however, is a complex function of source and environmental conditions especially windspeed (Bursik 2001) and relative humidity (Woods 1993; Glaze et al. 1997; Graf et al. 1999; Mastin 2007), so using plume height alone to estimate mass loading can lead to severe under- or overestimation of mass eruption rate. For weak plumes in high winds, for example, it is not possible to simply use column height to derive mass loading or MER, as modeling suggests that the estimated MER can be to two orders of magnitude too low (Bursik 2001; Bursik et al. 2009).

Rather than using a simplistic scaling relationship based on one-dimensional steady plume theory in the absence of a cross-flow or atmospheric water vapor, we use a numerical eruption column model that allows for more complex physics. One way to use such a model would be to obtain a better estimate of mass eruption rate from a measured eruption column height, and wind and relative humidity profiles (Fig. 2). Another way to use such a model is to estimate a mass eruption rate from any available measured conditions at the vent, such as vent radius, eruption speed or temperature, and the atmospheric profile. To explore the possibility of obtaining estimates of mass eruption rate using a numerical model that can take a variety of data inputs, we employ the model bent (Bursik 2001), which has been modified to incorporate volcano observations and then provide initial

**Fig. 2** Calculation and comparison of eruption column height and mass eruption rate for the paroxysmal phase of the April 2010 eruption. **a** Blue line is observed plume height (minimum observable about 2,500 m using IMO Doppler radar at Keflavik airport); black circles are calculated plume height with (bent) using IMO Keflavik radiosonde windspeed data (vertical colored bars) centered on nominal time of measurement (every 12 h). Windspeed color bar in meter per second. **b** Black circles are MER corresponding to bent plume heights calculated in (a); filled triangles MER from Sparks et al. (1997); open triangles MER from Mastin et al. (2009). For reference, data-points in part (b) are at the following coordinates: (10-04-14 12:00:00, 1.639E+06) (10-04-15 00:00:00, 9.8304E+06) (10-04-15 12:00:00, 7.03396E+06) (10-04-16 12:00:00, 3.326E+06) (10-04-17 00:00:00, 9.9434E+05) (10-04-17 12:00:00, 1.6067E+06) (10-04-18 00:00:00, 8.308E+05) (10-04-18 12:00:00, 5.244E+05). At 0Z 16 Apr 2010, the plume was below the detection limit of the Keflavik radar



conditions for the ash transport model puff. Using boundary conditions on eruption temperature and water vapor content, as well as grain size, crater diameter, and speed of erupting mixture (Table 1) coupled with atmospheric conditions as given by radiosonde data, bent solves a cross-sectionally averaged system of prognostic equations for continuity,

momentum, and energy balance. Variable parameters (such as density, gas constant, entrainment constant, etc.) are solved with a set of diagnostic equations. Bent takes a size distribution of pyroclasts, then outputs the mass distribution with height of the various sized clasts in the atmosphere. Bent results suggest that increasing wind speed causes

**Table 1** Uncertain eruption source parameters based on observations of the 2010 Eyjafjallajökull eruption and information from other eruptions of the past of the same type

Parameter	Value range	PDF	Comment
Vent radius, $b_0$ , m	65–150	Uniform, +definite	Measured from IMO radar image of summit vents on 15 April 2010
Vent velocity, $w_0$ , m/s	45–124	Uniform, +definite	Measured by infrasound 6–21 May, when MER similar to 14–18 April
Mean grain size (Folk and Ward 1957), $Md_{\varphi}$ , $\varphi$ units	2 boxcars <sup>a</sup> : 1.5–2 and 3–5	Sum of two uniform, $\in R$	(Woods and Bursik 1991), Table 1, vulcanian or phreatoplinian. A. Hoskuldsson, Eyjafjallajökull Eruption Workshop, 09/2010, presentation, quote: 'vulcanian with unusual production of fine ash'.
Grain size sorting, $\sigma_{\varphi}$ , $\varphi$ units	2.0±0.6	Uniform, $\in R$	(Woods and Bursik 1991), Table 1, vulcanian or phreatoplinian

<sup>a</sup> Boxcar: function that is zero everywhere except over a short interval where it is constant

enhanced entrainment of air and horizontal momentum, plume bending, and a decrease in plume rise height at constant eruption rate. Thus, it is able to model how wind and atmospheric stratification affect the plume rise height (Graf et al. 1999), and has been tested against plume rise height data, and against dispersal data (Bursik et al. 2009).

Given our use of a numerical eruption column model, we can take advantage of all potential data available for characterizing the volcanic source, such as satellite observations of eruption temperature and vent size, infrasound measurements of eruption speed, visual observations of plume or eddy rise or ballistic speed, visual observations of vent size, visual observations of column collapse, FLIR observations of eruption speed and temperature, radar observations of grain size, etc. In the present contribution, instead of using column height to get MER and mass loading, we use estimates of source variables (together with their uncertainties): initial (vent) exit speed and vent radius, and grain size (Table 1). Other important boundary conditions are those of temperature and water content (because of computational restrictions explained more thoroughly further in this contribution, both are assumed to be single-valued, and taken to have characteristic values of eruption temperature,  $T_{\text{eruption}}=1,200$  °C and source water vapor content,  $n_0=1.7$  wt.%; (Keiding and Sigmarsson 2012)) (see Supplement A for example bent input file).

For the start time and duration of the initial eruptive pulse, no more data are available than observations that the summit vent must have become active around midnight in the morning of 14 April 2010, and that the eruption continued at first light (Thorkelsson 2012). We therefore estimate that the eruption started at midnight, and use an ash transport and dispersal model default source eruption duration of 3 h. We have used radar measurements from 15 April 2010 to estimate vent size, and infrasound from the second strong eruptive phase in May 2010 to estimate vent velocity, but both variables have been estimated during other eruptions by a variety of methods. Most commonly, both vent size and ejection speed have been measured from ground-based observation or photography (Chouet et al. 1974; Sparks and Wilson 1982; Calder et al. 1997). From the source variables, bent can be used to calculate model MERs and plume heights. Below, we check these for consistency with observed plume height.

In producing its eruption outputs, bent accounts for atmospheric (wind, temperature, humidity, etc.) conditions as given by atmospheric sounding data. Thus plume rise height is given as a function of volcanic source *and* environmental conditions. To aid in the hindcast exercise herein, we make use of the IMO Keflavik radiosonde from 14 April 00Z. The radiosonde is the closest weather data both spatially and temporally to the early period of the eruption between about midnight and 07Z, and therefore best represents the near-vent weather conditions.

The volcanic source variables estimated for our computations (Table 1) resulted in output eruption column model heights varying between the top of the volcano at 1.7 km ASL and 8 km (Figs. 2 and 3), and grain size distribution at height of  $Md_\varphi$  ranging from  $1.5 < \varphi < 5$ , and  $\sigma_\varphi$  from  $0.4 < \varphi < 4.8$ . (The  $\varphi$  size system is defined as  $\varphi = \log_2(d/d_0)$ , where  $d$  is grain size in millimeters, and  $d_0=1$  mm; moments are calculated by mass, not by particle count.) The model column heights are consistent with the observations noted above of column collapse accompanying sustained eruption columns, as well as column heights measured from the Keflavik radar data. The radiosondes for much of the initial phase of the eruption (14–18 April) generally show a marked peak in wind speed at altitudes between 5 and 10 km, with  $v$ , of 30–60 m/s; this finding is consistent with the jetstream flowing almost directly over Eyjafjallajökull. We found that, although the input parameter values used in the plume model produced a plume that rose to 1.7–8 km, for many input values the plume rise height would have been much higher and is in this range owing to a shearing of the plume by the jetstream (Fig. 2). The calculated MER drops off exponentially with time in the first days of the eruption. Given this exponential drop-off as well as the heavy ash loading from the initial eruptive phase, we speculate that the initial MER was likely greater than  $10^7$  kg/s. Because of the interaction of the plume with the wind, there is disparity in MER (hence loading) between the bent estimate and the scaling relationships, of up to two orders of magnitude.

The output from bent is put in a file that initializes a puff run, which consists of information on ash loading and grain size distribution as a function of height and other geometric parameters dealing with plume shape (Supplement A).

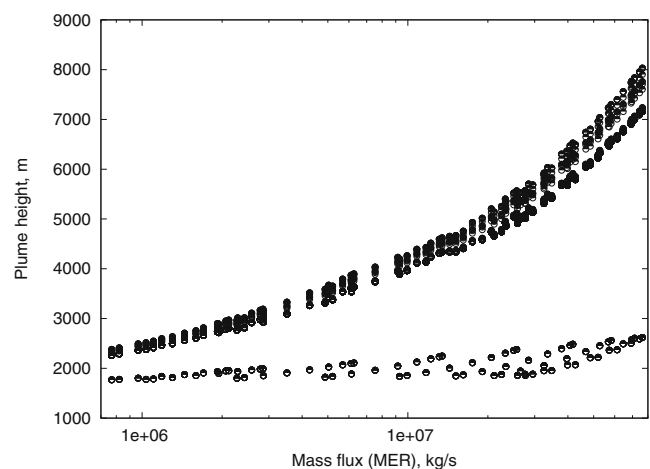


**Fig. 3** Mass fluxes determined by the eruption source conditions (Table 1) using bent and IMO radiosonde data ranged from  $\sim 7 \times 10^5$  to  $\sim 7 \times 10^7$  kg/s, resulting in occasional eruption plume (column) collapse (lower grouping of output points)

Given these initial conditions for ash transport produced by bent, the puff Lagrangian VATD model was used to propagate ash parcels in a wind field (Searcy et al. 1998). Puff tracks a finite number of Lagrangian point particles of different sizes, whose location  $R$  is propagated from timestep  $k$  to timestep  $k+1$  via an advection/diffusion equation

$$R_i(t_{k+1}) = R_i(t_k) + W(t_k)\Delta t + Z(t_k)\Delta t + S_i(t_k)\Delta t \quad (1)$$

Here  $R_i(t_k)$  is the position vector of the  $i$ th particle at time  $k\Delta t$ ,  $W(t_k)$  is the local wind velocity at the location of the  $i$ th particle,  $Z(t_k)$  is a turbulent diffusion that is modeled as a random walk, and  $S_i(t_k)$  is a term which models the fallout of the  $i$ th particle due to gravity. Note therefore that puff takes into account dry particle fallout (not wet fallout or aggregation, in common with most VATD models), as well as dispersion and advection. For more detailed description see Searcy et al. (1998); source code and documentation is available at <http://puff.images.alaska.edu/monitoring.shtml>. Puff can be run using one of several numerical weather prediction windfields (NCEP 2009a; NCEP 2009b; USN-FNMOC 2009; WRF 2009). These NWP models are available at differing levels of spatial and temporal resolution. In the present case, puff uses global NCEP/NCAR reanalysis windfields to track the propagation of ash from Iceland to Europe, using 6-h,  $2.5^\circ$  data. Outputs from a deterministic puff model run consist of ash parcel positions and smoothed concentration fields. The outputs can be post-processed to extract outcomes like maximum height of ash, which can be compared to observations.

### Methodology of uncertainty quantification

A comprehensive accounting for the many uncertainties in model outputs can be represented in different ways, including: (1) worst-case scenarios that attempt to provide bounds using interval analysis (Ben-Haim and Elishakoff 1990; Natke and Ben-Haim 1997); (2) methods based on fuzzy set theory, linguistically often identified as being concerned with possibility (Elishakoff 1999); (3) evidence theory, which tries to create upper and lower bounds on the likelihood of events (Shafer 1976); and (4) probabilistic or stochastic models, which offer a mathematically rich structure (Adler 1981; Augusti et al. 1984; Christakos 1992; Grigoriu 2002; Papoulis 1984; Torquato 2002). As the existence of several approaches suggests, there is no “best” approach to quantifying uncertainty, even within a specific scientific problem.

To account for the parametric (input) uncertainties in a model, one can use available data and expert knowledge to formulate a probability distribution function (pdf) of the inputs and then evaluate the model with sufficiently many different inputs using a Monte Carlo sampling technique. In

the standard puff model with turbulence turned off used herein, one tracks the position of representative particles as they are transported by wind, and the position of each parcel is a deterministic quantity. Each puff simulation consists of the transport of millions of such parcels. The resultant set of outputs and functionals of outputs (e.g., maximum height of the ash cloud at a given location from each run of puff) can be treated as a data set and analyzed to establish a pdf of the desired output or compute appropriate statistics (means, medians, and variances). Unfortunately, even for simple choices of the input variables the computational cost of this approach—requiring millions of model evaluations—is soon unaffordable. To alleviate this cost yet produce a solution in which the statistical moments of the outputs converge, we create a small, “smart” combination of simulations consisting of thousands of runs, as opposed to a Monte Carlo combination consisting of millions of runs. The outputs can be combined to produce results comparable to those from a Monte Carlo procedure but at a much smaller computational cost. This procedure has origins dating back to the work of Wiener (1938), and has been the subject of much recent study (see for e.g., Xiu and Karniadakis (2002), LeMaitre et al. (2001), Xiu and Hesthaven (2005), and Berveiller et al. (2006)). Such a methodology for block and ash flows was presented in detail in an earlier work (Dalbey et al. 2008), and is extended here for the current application to ash transport.

### Uncertainty characterization

Given the paucity of information about the intensity of the eruption during its strongest, early morning initial phase, we use available information to construct a constant source-time function of steady output in mass eruption rate and grain size for the puff default eruption duration of 3 h, initializing the eruption at midnight, 14 April 2010. Each instance of the source-time function is constructed from a single sample of the space of uncertain bent input parameters gleaned from the best available information for this and other similar eruptions. The grain size, mass loading and ash cloud height, width, and depth output from bent are then taken as input to the VATD model puff. In addition to the (uncertain) volcanic source inputs, a VATD model such as puff requires NWP wind data that are subject to temporal and spatial variation that is not captured by available datasets. With this proviso—that the wind is also an important source of uncertainty that we are not in the present case characterizing, we proceed to propagate the uncertainty derived from our lack of complete understanding of the volcanic source characteristics. Furthermore, we mention explicitly that, although we have employed bent and puff models in this paper, our analysis is not dependent on these specific column and transport models. Other models for either the volcanic eruption column or the VATD process

could be used instead, and, following the same methodology, would produce a similar probabilistic forecast of ash cloud location.

Polynomial chaos quadrature weighted estimate

Consider any output variable of interest (e.g., ash concentration at a location). We assume this to be a random variable,  $x_k$ , whose time evolution is given by the bent-puff coupled eruption column advection/diffusion solver, written as a generic differential equation

$$\dot{x} = f(t, x, \Theta, \mathcal{W}) \tag{2}$$

In Eq. 2,  $t$  is time,  $\Theta = \{\theta_1, \theta_2, \dots\}$  represents uncertain system parameters such as the vent radius, vent velocity, mean grain size, and grain size variance, and  $W$  is a given windfield from a NWP model. As noted above,  $\mathcal{W}$  is indeed also stochastic, and its uncertainty may be expressed using ensembles of possible windfields (WRF 2009). We focus here on the effect of the volcanic source parameter uncertainty, conditional to a given windfield forecast. We intend to incorporate the effect of the wind uncertainty in upcoming contributions using an extension of the present methodology.

Using the estimated values of physical variables of vent speed and radius and grain size distribution, together with estimates of their uncertainty, as inputs into the bent eruption column model, we generate a sampling of the uncertain input parameter space for a typical VATD model. From this sample of puff runs, we then generate statistical moments for any output variable of interest, such as concentration at a point or in a region, or cloud size and position. In the present case, the output variables that we will concentrate on are related to ash cloud size and position, as measurements of these parameters from satellite data are better—having a longer history of development and testing—than are measurements of concentration, and therefore more suitable for model comparison and validation.

The starting point for our development of the PCQWE method is to approximate the input and output variable distributions by a truncated polynomial series, the polynomial being associated with the distribution (so, e.g., the Hermite polynomials are associated with a Gaussian distribution):

$$\theta_i(\xi) = \sum_{k=0}^N \theta_{ik} \phi_k(\xi) = \Theta_i^T \Phi(\xi) \Rightarrow \Theta(t, \xi) = \Theta_{pc} \Phi(\xi) \tag{3}$$

$$x_i(t, \Theta) = \sum_{k=0}^N x_{ik}(t) \phi_k(\xi) = x_i^T(t) \Phi(\xi) \Rightarrow x(t, \xi) = \mathbf{X}_{pc}(t) \Phi(\xi) \tag{4}$$

where,  $\mathbf{X}_{pc}$  and  $\Theta_{pc}$  are matrices composed of coefficients of PC expansions for state  $\mathbf{x}$  and parameter  $\Theta$

respectively and  $\{\phi_k\}$  is the set of orthogonal polynomials in the unit random variable  $\xi$  chosen for the approximation. This approach was pioneered by Xiu and Karniadakis (2002) and termed generalized polynomial chaos (gPC). gPC is an extension of the homogeneous chaos idea of Wiener (1938) and involves a separation of random variables from deterministic ones in the solution algorithm for a stochastic differential equation. Suitably chosen polynomials converge rapidly to the assumed pdf for the input variables.

Galerkin projection (multiplication by  $\phi_k$  and integration over  $dp(\omega)$ , where  $p$  is probability and  $\omega$  is a dummy variable that spans the random space) is used to generate a system of deterministic differential equations for the expansion coefficients. The Galerkin projection step fails when applied to problems with non-polynomial nonlinearities, and can produce unphysical solutions when applied to systems modeled by hyperbolic partial differential equations. Furthermore, Galerkin projection requires that a “new” set of unphysical partial differential equations be solved—a difficult option since the primary models bent and puff cannot be easily altered. Non-intrusive spectral projection (NISP) or stochastic collocation methods can overcome these difficulties (LeMaitre et al. 2001; Xiu and Hesthaven 2005; Berveiller et al. 2006). Dalbey et al. (2008) have proposed polynomial chaos quadrature (PCQ) as a variation of the NISP method (see LeMaitre et al. (2001), Xiu and Hesthaven (2005), and Berveiller et al. (2006)). Key to this methodology is the recognition that the projection desired to estimate the coefficients of the polynomial expansion or to estimate moments (mean, variance, etc.) will require numerical integration with quadrature of the state variable  $\mathbf{x}$ , using the numerical integration of the expression for the time derivative of  $\mathbf{x}$  from Eq. 2. PCQ approximates the  $N$ th moment of  $\mathbf{x}$  as:

$$\langle \mathbf{x}(t)^N \rangle = \int_{\Omega} \left( \int_0^t \dot{\mathbf{x}} dt \right)^N dp(\omega) = \int_{\Omega} \left( \int_0^t f(t, \mathbf{x}, \Theta, \mathcal{W}) dt \right)^N dp(\omega) \tag{5}$$

$$= \sum_q w_q (f(t, \mathbf{x}, \Theta_q, \mathcal{W}))^N \tag{6}$$

For a fixed value of parameter  $\Theta = \Theta_q$ , the evaluation of  $\mathbf{x}$  is done using a run of bent and puff. This method can be viewed as a Monte Carlo-like evaluation of system equations, but with sample points  $\xi_q$  and corresponding weights  $w_q$  selected by quadrature rules. In other words, the output moments are approximated as a weighted sum of the

output of simulations run at carefully selected values of the uncertain input parameters (namely the quadrature points). The formula above for moments can be used to estimate the means and variances. Similarly the  $i$ th polynomial coefficient for the  $k$ th random variable,  $x_{ik}$ , can be obtained as,

$$x_{ik} = \frac{\sum_q w_q f(t, \mathbf{x}, \Theta_q, \mathcal{W}) \phi_i(\xi_q)}{\sum_q w_q (\phi_i(\xi_q))^2} \quad (7)$$

With the coefficients in hand, the truncated polynomial series can be used to estimate probabilities. The Gaussian quadrature points optimize the degree of the polynomial function that integrates exactly an Hermite polynomial representation of the uncertainty. The classic method of Gaussian quadrature exactly integrates polynomials up to degree  $2N+1$  with  $N+1$  quadrature points to obtain the  $N$ th moment. The tensor product of one-dimensional quadrature points is used to generate quadrature points in general  $n$ -dimensional parameter space. As a consequence, the number of quadrature points increases as  $(N+1)$  to integrate exactly an  $n$ -variate polynomial of degree  $2N+1$  as the number of uncertain input parameters,  $n$ , increases. Thus, in the analysis below, when we use  $9^4=6,561$  quadrature points (model runs), it means that there are four uncertain input parameters (vent radius, vent velocity, initial mean grain size, and initial standard deviation of the grain size) for which we are integrating the polynomials up to degree 17 ( $=2 \times 8+1$ ) and are able to calculate moments up to order 4. It is important to point out here the extremely sensitive dependence of the number of quadrature points on the number of uncertain parameters, i.e., the number of points goes up in proportion to the *power* of the number of parameters. This effectively limits the number of uncertain input parameters that can be propagated. For example, although four variable input parameters necessitate about  $10^4$  model runs in the present case, eight variable input parameters necessitate  $10^6-10^7$  runs. Thus, one needs to be judicious and parsimonious in the choice of only the most critical input parameters that are to have variability. Although the present contribution cannot include a sensitivity study of the relative importance of various uncertain input parameters, we have tried to wisely choose those four that should have the most profound impact on the output mass and geometry. The input source variables deemed to have the most direct impact on cloud geometry and loading are vent radius, source vent velocity, initial grain size mean, and initial grain size standard deviation. Vent radius and source vent velocity directly control mass eruption rate, hence column height and spreading. Initial grain size mean and standard deviation are the source

conditions that most directly control the fallout rate of the particles, hence the mass loading at the height of the eruption cloud.

## Analysis and PCQWE results

The first step in the analysis is to produce the sampling values and their weights, for the uncertain bent inputs, viz. vent radius, vent velocity, mean grain size, and grain size variance. The inputs are sampled at selected points, in the present case, Gauss-Legendre quadrature points, since the underlying distribution has been taken to be uniform for each of our uncertain inputs. We have used uniform distributions as given data consist only of ranges. We cannot assign to any one point within each range a higher likelihood than surrounding points. Outputs are summed with appropriate weights, producing the polynomial chaos quadrature weighted estimate of downwind ash position and loading. For the range of values of vent radius and velocity that were sampled, we noted two different regimes of plume rise (Fig. 3); the lower regime is associated with those inputs that result in eruption column collapse. As noted previously, at least partial column collapse seemed to be a major feature of this eruption.

Since PCQ is a numerical method of integration ( $\int_{\Omega} f(x)dx \approx \sum_{i=1}^{N_q} w_i f(\xi_i)$  where  $N_q$  is the number of quadrature points and  $w_i, \xi_i$  are quadrature point and weight combinations), using an insufficient number of quadrature point-driven samples will result in integration error. This necessitates an adaptive or nested quadrature scheme that allows us to successively refine the accuracy by increasing the number of sample points, i.e., simply running the model at additional quadrature points rather than having to resample the input distributions. In a nested quadrature scheme, one can compare the solution computed at a given order with that of a quadrature rule of lower order, which evaluates the integrand at a subset of the original  $N$  points, to minimize the integrand evaluations. Gaussian quadrature rules are not naturally nested. Hence, we employ Clenshaw–Curtis quadrature (Cheney and Kincaid 1999; Clenshaw and Curtis 1960) for numerical integration. The Clenshaw–Curtis scheme is based on an expansion of the integrand in terms of Chebyshev polynomials and naturally leads to nested quadrature rules. Another advantage of Clenshaw–Curtis quadrature is that the quadrature weights can be evaluated in order  $M \log N$  time by fast Fourier transform algorithms as compared to order  $N^2$  for the Gaussian quadrature weights.

Following runs of bent at the quadrature points, each output is then propagated through puff, which was then run for a real-time period of 5 days. The weighted outputs from puff were then combined to produce a probabilistic



estimate of ash cloud position by applying the appropriate weight to each deterministic bent-puff run.

Numerical methodology of the type used here must always be tested for independence from discretization parameters and number of model runs. As we seek to develop a numerical method that could be implemented in a finite (usually short) computing time, we need to minimize the number of puff particles used and the total number of runs, while at the same time maintaining model accuracy. The number of model runs is given by the number of quadrature points. Convergence of moments in PCQ as a function of the number of quadrature points is discussed in detail in (Dalbey et al. 2008). For the present set of simulations, we compared the outputs for  $9^4=6,561$  model runs against those for  $13^4=28,561$  model runs (quadrature points). The results indicate that  $9^4$  runs is substantially the same as  $13^4$  runs in terms of the values of selected outputs (Fig. 4). In examining the output ash cloud top height for 16 April 2010 12Z, for 6,047 computational grid points, the maximum deviation between  $9^4$  and  $13^4$  quadrature points is 2.76 %, and the mean difference is 0.02 %. For this analysis, percent differences were calculated by normalizing the cloud top height difference between  $9^4$  and  $13^4$  quadrature points against the maximum cloud height at the given time. Most grid points contain no ash in both model runs, thus the difference between the mean and maximum deviations. These results suggest that  $9^4$  runs is sufficient for propagation of the uncertainty in the inputs. In terms of sensitivity to discretization parameters, the most important discretization in puff is the use of Lagrangian “particles” that are propagated in the windfield. Once the particles have been

moved sufficiently far, they need to be counted in some way to obtain smooth concentration gradients as one sees in nature. If too few particles are used, then the smoothing process can yield poor estimates of concentration as a function of position. In terms of the effect of discretization parameters, the comparison of outputs using  $10^5$  to  $10^7$  particles in the puff simulation indicated that the choice of  $4 \times 10^6$  particles was adequate for our purposes (Table 2), and is consistent with the findings of others (Scollo et al. 2011).

We focus on four-dimensional ash cloud-top position in presenting typical output from this process, as this will be our validation dataset as well. Results for  $9^4$  Clenshaw–Curtis quadrature points and  $4 \times 10^6$  puff particles for 16 April 2010 are shown in Fig. 5. Although maximum mean ash cloud-top height hovers between 1 and 2 km, the standard deviation in the estimate is higher, and the region of non-zero deviation is much larger than that of the mean. Thus, the standard practice of capturing most of the probability density or mass by taking the mean plus three standard deviations of an output variable (encompassing approximately 99.7 % of the probability mass, assuming a Gaussian distribution of the output variable) will result in a maximum predicted cloud-top height of approximately 8 km at these times. One can conclude from this that the input source parameter uncertainty resulted in a sufficiently large uncertainty in downwind ash cloud position. Clearly, this result shows that it is critical to do everything possible to “beat down” the input source parameter uncertainty if we are to obtain tightly constrained estimates of the position of the downwind ash cloud, but that even what might be a poorly constrained estimate is helpful.

### Discussion and conclusions

For model evaluation and validation, both individual deterministic puff runs and PCQWE output were compared with

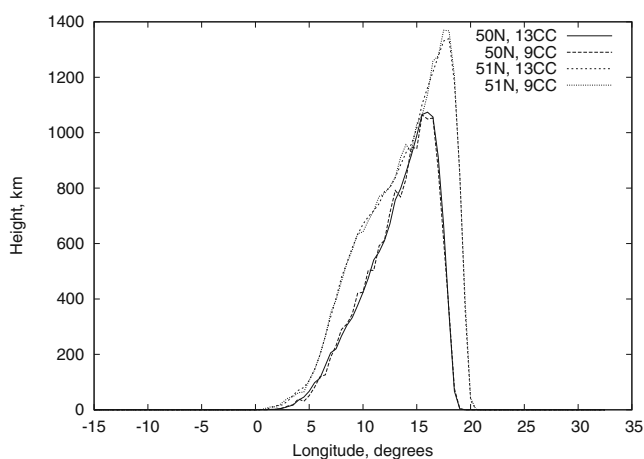


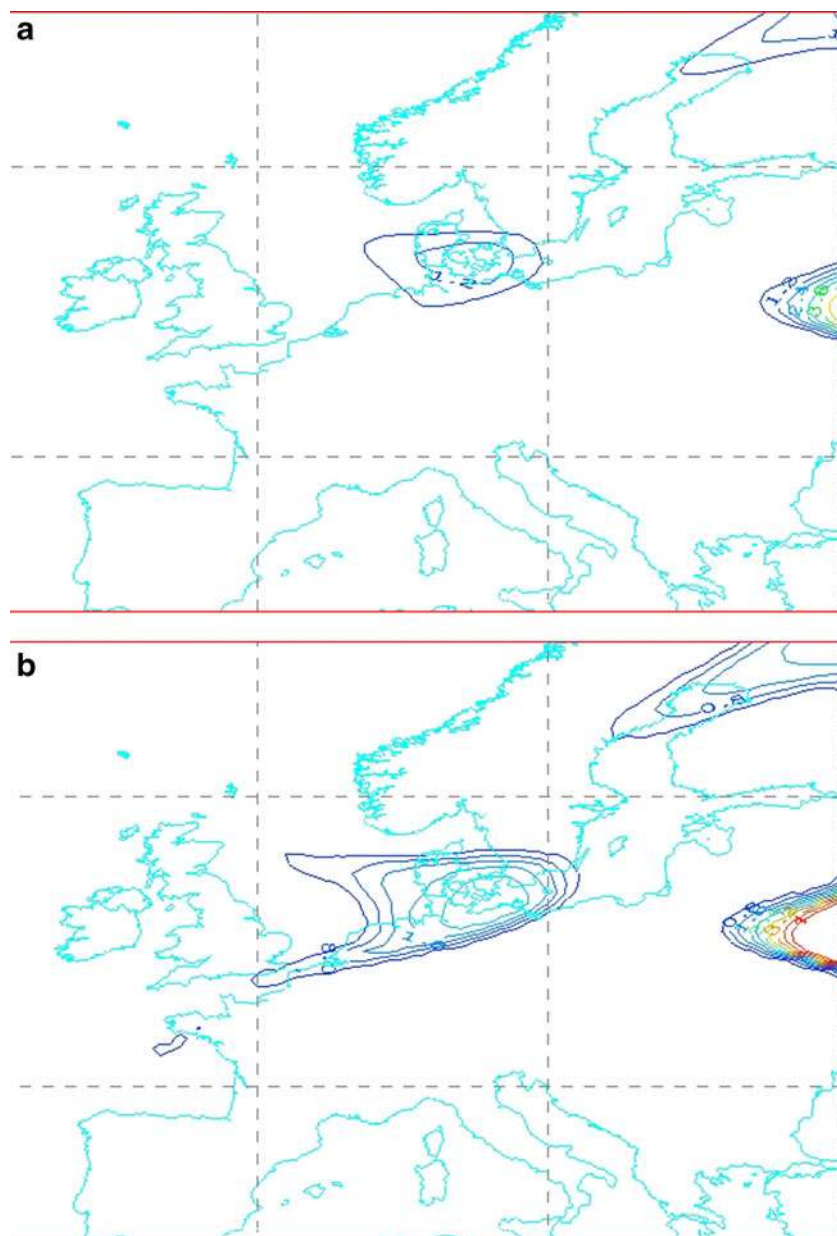
**Fig. 4** Comparison of output on mean cloud-top height from runs of  $9^4$  and  $13^4$  quadrature points, taken as transects along latitudes 50 and  $51^\circ$  North. Each curve is labeled according to the number of runs and the latitude. Comparison is between the runs having different numbers of quadrature points along the same parallel

**Table 2** Comparison of concentration at  $52^\circ$  N,  $13.5^\circ$  E and 0–2,000 m elevation using different numbers of initial puff particles

$n$ puff particles (initial)	Abs. concentration ( $\text{mg}/\text{m}^3$ )	Rel. concentration (puff particles in cell)
$1 \times 10^5$	$1.15 \times 10^{-3}$	28
$5 \times 10^5$	$1.82 \times 10^{-3}$	221
$1 \times 10^6$	$1.66 \times 10^{-3}$	405
$2 \times 10^6$	$1.74 \times 10^{-3}$	844
$4 \times 10^6$	$1.70 \times 10^{-3}$	1,655
$8 \times 10^6$	$1.79 \times 10^{-3}$	3,471
$1 \times 10^7$	$1.71 \times 10^{-3}$	4,151

The absolute concentration is calculated from the relative concentration assuming a cloud thickness of 1 km based on CALIOP data (e.g., Fig. 6)

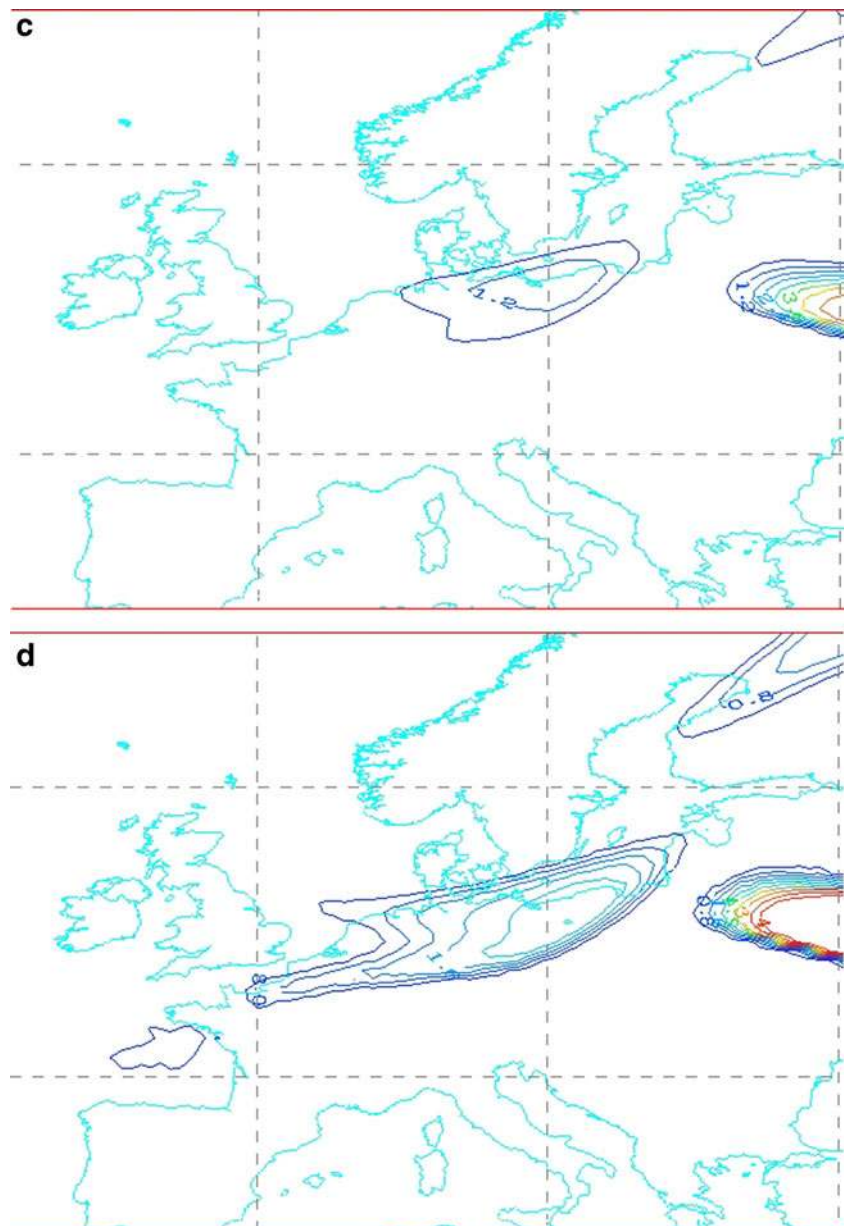
**Fig. 5** Model outputs for the ash cloud over north-central Europe on 16 April 2010 using  $9^4$  Clenshaw-Curtis quadrature points and  $4 \times 10^6$  puff particles. Ash cloud heights in meters; contour interval 600 m for mean and 400 m for standard deviation. **a** Mean cloud height at 00Z, **b** standard deviation of cloud height at 00Z, **c** mean cloud height at 06Z, **d** standard deviation of cloud height at 06Z, **e** mean cloud height at 12Z, **f** standard deviation of cloud height at 12Z, **g** mean cloud height at 18Z, and **h** standard deviation of cloud height at 18Z



ash position as determined by analysis of Meteosat-9 SEVIRI data. The main metric used in the present work is ash cloud-top height as a function of map position and time. Four-dimensional ash cloud top position on 16 April 2010 has been chosen for validation as it is thought to be well-characterized by the test dataset from Meteosat-9 SEVIRI. The plume generated in the initial, paroxysmal phase of the eruption in the early morning of 14 April 2010 drifted over northern Europe on 16 April 2010, hence this is the region and time we focus on. Meteosat processing by the algorithms used in this contribution is the most robust methodology for ash detection and assessment. Volcanic ash was identified in the satellite data using the methodology described in Pavolonis et al. (2006) and Pavolonis (2010). The ash loading (mass per unit area) and ash cloud height were

retrieved using an optimal estimation approach (Heidinger and Pavolonis 2009; Heidinger et al. 2010). Ash loading was not used for validation however as the SEVIRI data product consists of an estimate for an unknown depth within the upper part of the ash cloud. All microphysical assumptions used in the retrieval are described in (Wen and Rose 1994). In model and data, plume edge was defined by detectability of ash in a computational cell or pixel, respectively. Comparison with CALIOP limb sounder data suggests that Meteosat generally characterizes cloud top height well, but there are exceptions (Fig. 6). Volcanic ash cannot be detected if ash is obscured (from the top) by liquid water or ice clouds. This is true for all satellite-based infrared ash retrieval schemes. Based on careful manual analysis of satellite imagery, volcanic ash was generally the highest

Fig. 5 (continued)



cloud layer over Europe on 16 April 2010. However, higher level ice clouds did interfere with satellite detection of volcanic ash in areas northeast of Poland on 16 April 2010.

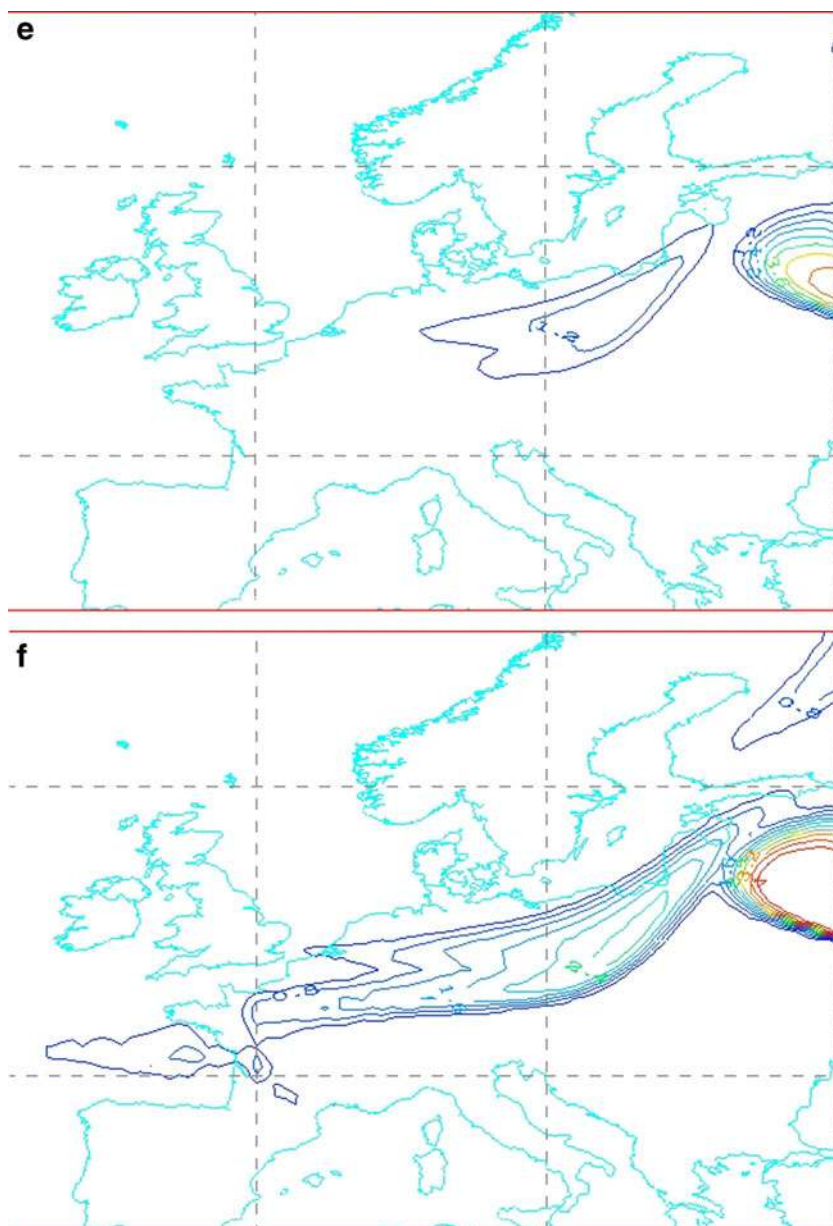
#### Qualitative comparison

In a qualitative analysis, PCQE ash location matches ash location in the data (Fig. 7). The Meteosat-9 SEVIRI cloud top height outputs were compared with model mean ash parcel height plus three standard deviations (statistics calculated from outputs of computational runs), as an estimated upper bound on predicted plume top height.  $9^4$  PCQ Clenshaw–Curtis runs were sampled in the input space, and  $4 \times 10^6$  ash particles were used. For a Gaussian, univariate distribution, mean  $\pm 3\sigma$  incorporates 99.7 % of the

model probability mass. Since in the present case pdfs are non-Gaussian, this value is somewhat lower. If we can assume that the largest values of vent radius and eruption speed resulted in the runs in which ash was transported at the highest modeled levels, this result suggests that the initial eruption was at the higher end of the intensities used in individual model runs. This would imply that the MER during the initial phase of the eruption was on the order of  $10^8$  kg/s.

None of a random sample of seven of the 6,561 model runs that went into the PCQE composite yielded ash parcels over northern Germany as seen in the SEVIRI test dataset. Thus, there is a non-zero probability mass of model runs that is encompassed by the space of reasonable estimated volcanic input source parameters, which contribute nothing to the

Fig. 5 (continued)

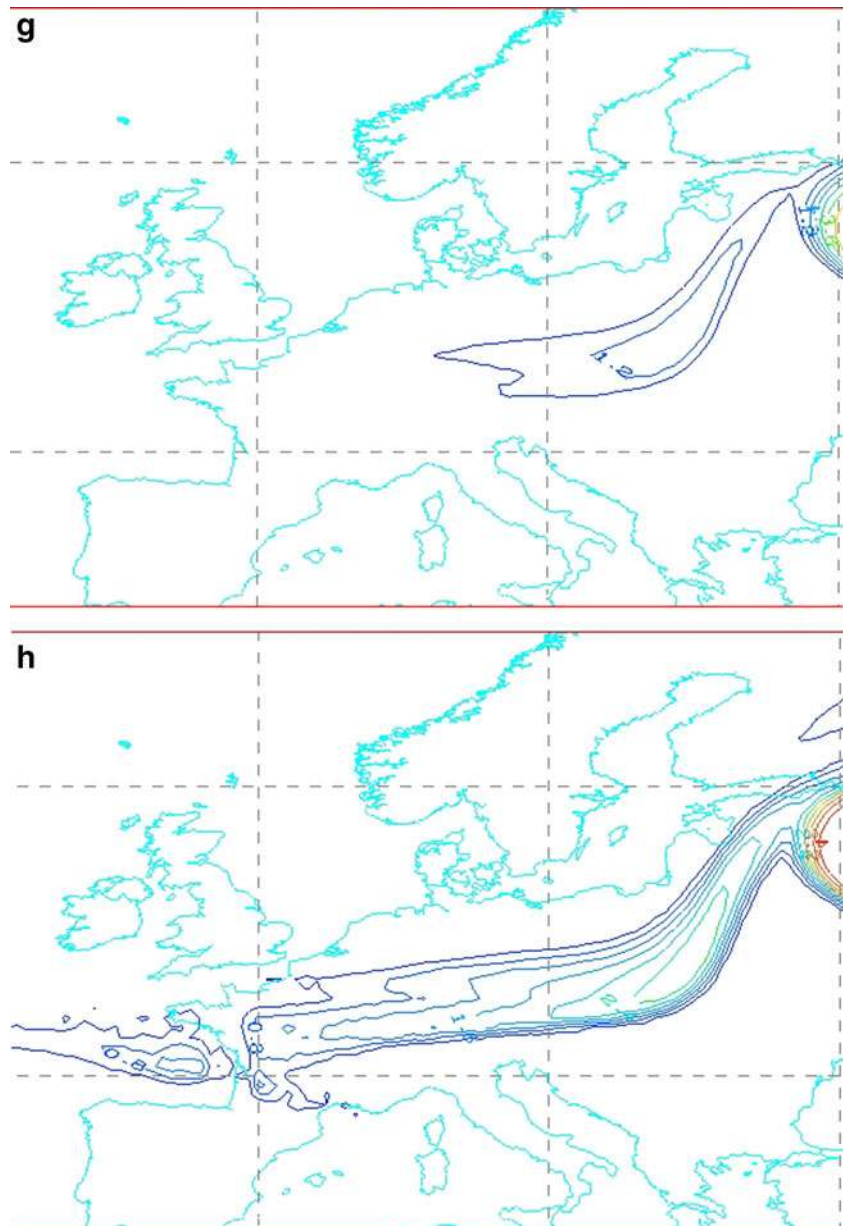


presence of ash in the forecast region. This suggests that individual runs of VATD models can yield results far from truth, even for rational choices of input parameters, and that stochastic combination is critical when volcanic input parameters are poorly constrained.

Continuing with our qualitative analysis, in planview, PCQWE predictions of location encompass a much larger area than does the data, but include most of the cells in which SEVIRI recorded ash. In both model and data, ash cloud top height varies from <1 km to c. 8 km. There is a variation in height along the axis of the ash cloud in the satellite data that in magnitude, and often in detailed location, corresponds with the variation seen in the PCQWE output (Fig. 7c–d), although the height variation does not correlate in detail at all times (Fig. 7a–b). (We note that comparison of SEVIRI ash

retrievals with CALIOP limb sounder data shows that these height variations are real.) Depending on the time, the position of the higher parts of the ash cloud in the satellite data shifts between its eastern and western ends. Locally, Meteosat can misinterpret meteorological clouds as ash clouds, and can have a larger variance in the vertical dimension than limb sounder data. These, as well as a poorly constrained vertical dispersion in the ash motion used in the model may contribute to this difference in height between model and data. Nevertheless, the point here is that since we do not know a priori the characteristics of the paroxysmal eruption column, the fact that the highest model ash parcels are close to the data suggests not only that the model parameter space encompasses the true, but that the paroxysmal initial pulse was as large as allowed by the parameter space.

Fig. 5 (continued)

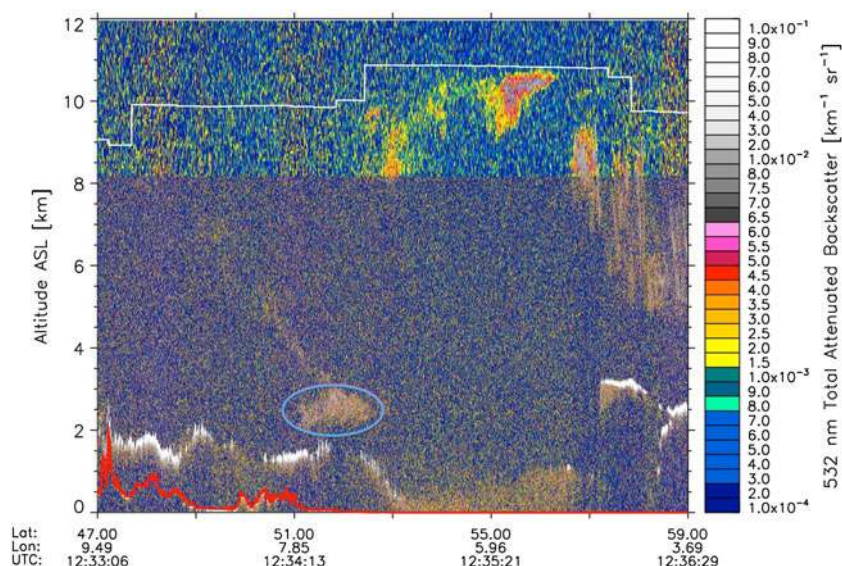


An important difference between model and data is the existence of ash clouds in the model to the northeast that are not present in the data. Detailed investigation of individual model runs shows that these ash bodies are derived in virtually all model runs at high elevation at a location west of Norway where the ash cloud bifurcates. The low-level ash cloud that corresponds to that seen in the Meteosat data propagates to the south from this point, while the high-level model cloud propagates eastward, eventually doubling back over Russia and northern Europe. Although there is no indication of such a cloud in the Meteosat data, as stated previously our detailed analysis of the satellite data suggests that higher level ice clouds did interfere with satellite detection of volcanic ash in areas northeast of Poland on 16 April 2010.

#### Quantitative comparison

Quantitative comparison of the probabilistic forecast of four-dimensional location calculated with PCQWE and Meteosat-9 was undertaken using data and output for 12Z 16 April 2010 for the ash cloud over north-central Europe (Table 3; Fig. 8). In Table 3, the Figure of Merit in Space and other statistics are calculated for each time for the correspondence in three dimensions between the PCQWE output mean ash cloud-top height plus three standard deviations (thus encompassing about 99.7 % of the probability mass) and the ash cloud-top height as given by the Meteosat-9 SEVIRI retrieval. The most general statement that can be made is that PCQWE output includes the entire Meteosat-9 ash cloud area at the 5 % level (i.e., in the figure,

**Fig. 6** CALIOP space-borne lidar detection of the Eyjafjalajökull ash cloud over northern Europe on 16 April. *White line* is elevation of tropopause; *red line* is elevation of ground surface. The discontinuity at 8.5 km altitude is due to a change in the vertical and horizontal resolution of CALIOP, which changes the noise characteristics of the data. The *blue oval* outlines the ash layer. Near this location and time, the highest ash was detected by Meteosat at c. 3 km, with considerable altitudinal variation down to c. 100 m



95 % of the model probability mass is inside the appropriately colored region that completely encompasses the data), and that model and data correspond quite well even at the 70 % level (i.e., 30 % of the probability mass encompass most of the data). Table 3 shows that when using the

standard measure of mean plus three standard deviations in ash cloud location, at best PCQWE predicts location with around 83 % probability (“PCQWE given Sat” row in the table). This result is sensitive to the lower elevation cutoff used in PCQWE. In the two cases studied, when the

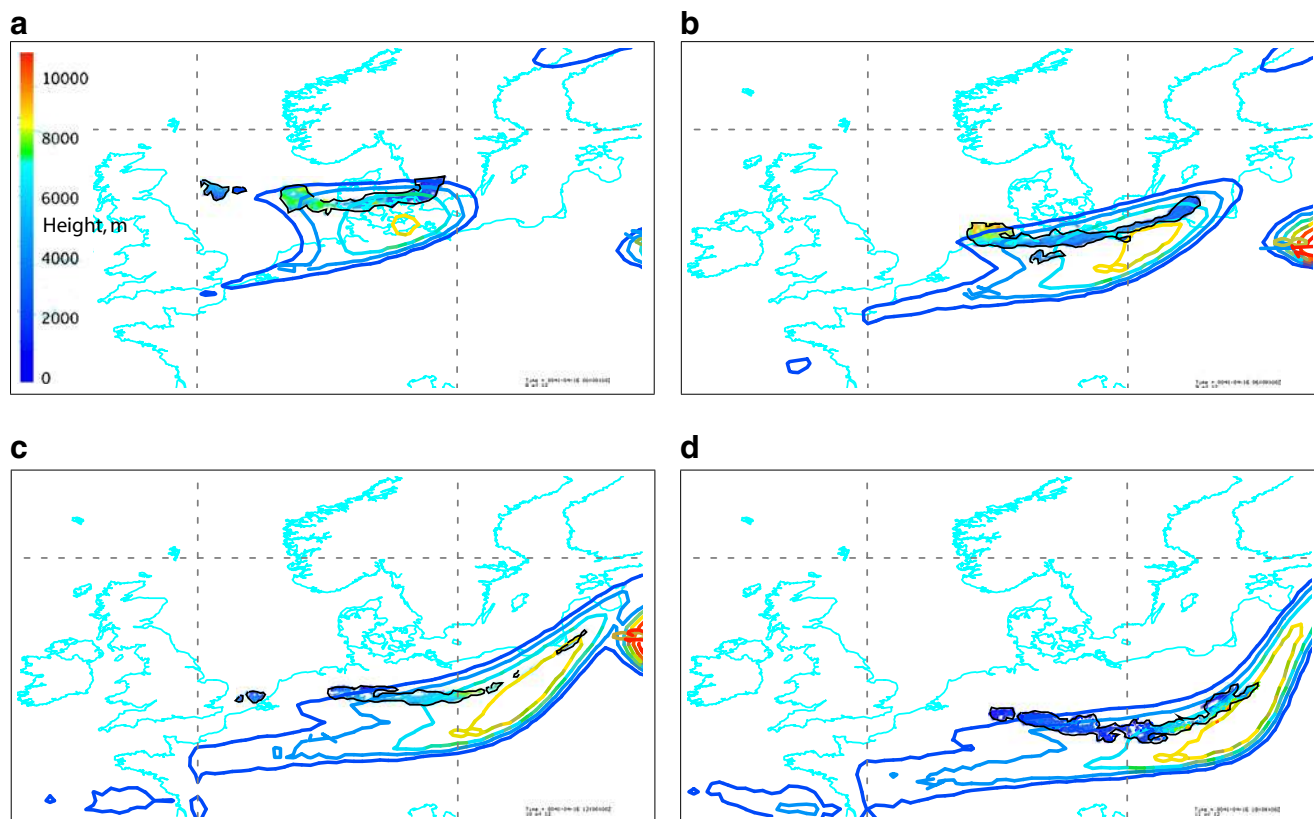


**Fig. 7** Meteosat-9 SEVIRI cloud top height data product compared with model mean ash parcel height plus three standard deviations. Colored regions are SEVIRI cloud top estimate; contours of cloud height are model. Outermost contour is 2,000 m height and contour

interval is 2,000 m. There is a  $\pm 1$  km quantization error in the model height output. **a** 16 April 2010 00Z, **b** 16 April 2010 06Z, **c** 16 April 2010 12Z, **d** 16 April 2010 18Z

**Table 3** Comparison of forecast for April 16 at 12Z and satellite data using  $4 \times 10^6$  puff particles and  $9^4$  and  $13^4$  points of Clenshaw–Curtis quadrature rule-based PCQWE

Metric of footprint	PCQW min ht 124 m* $9^4$ points	PCQWE min ht 124 m $13^4$ points	PCQWE min ht 380 m* $9^4$ points	PCQWE min ht 380 m $13^4$ points
FMS	0.0544	0.0553	0.0690	0.0715
PCQWE given Sat	0.8238	0.8268	0.6889	0.6879
Sat given PCQWE	0.0551	0.0559	0.0712	0.0739

Mean +3 standard deviations used for forecast; 380 m is default lowest quantization of heights in Meteosat data in software used in calculation; 124 m is minimum height in Meteosat ash top height data on 16APR at 12Z

*FMS* figure of merit in space = (area of intersection of PCQWE forecast and satellite image)/(area of union), *PCQWE given Sat* = (area of intersection PCQWE forecast and satellite image)/(area of satellite), *Sat given PCQWE* = (area of intersection PCQWE forecast and satellite image)/(area of PCQWE forecast)

**Fig. 8** Meteosat-9 SEVIRI cloud outline (filled black region) compared with model generated probabilities of ash presence based on source parameter uncertainty propagation. Color scale bar in fractional probability. Outer edge of blue area is at 20 % probability. **a** 16 April 2010 00Z, **b** 16 April 2010 06Z, **c** 16 April 2010 12Z, **d** 16 April 2010 18Z

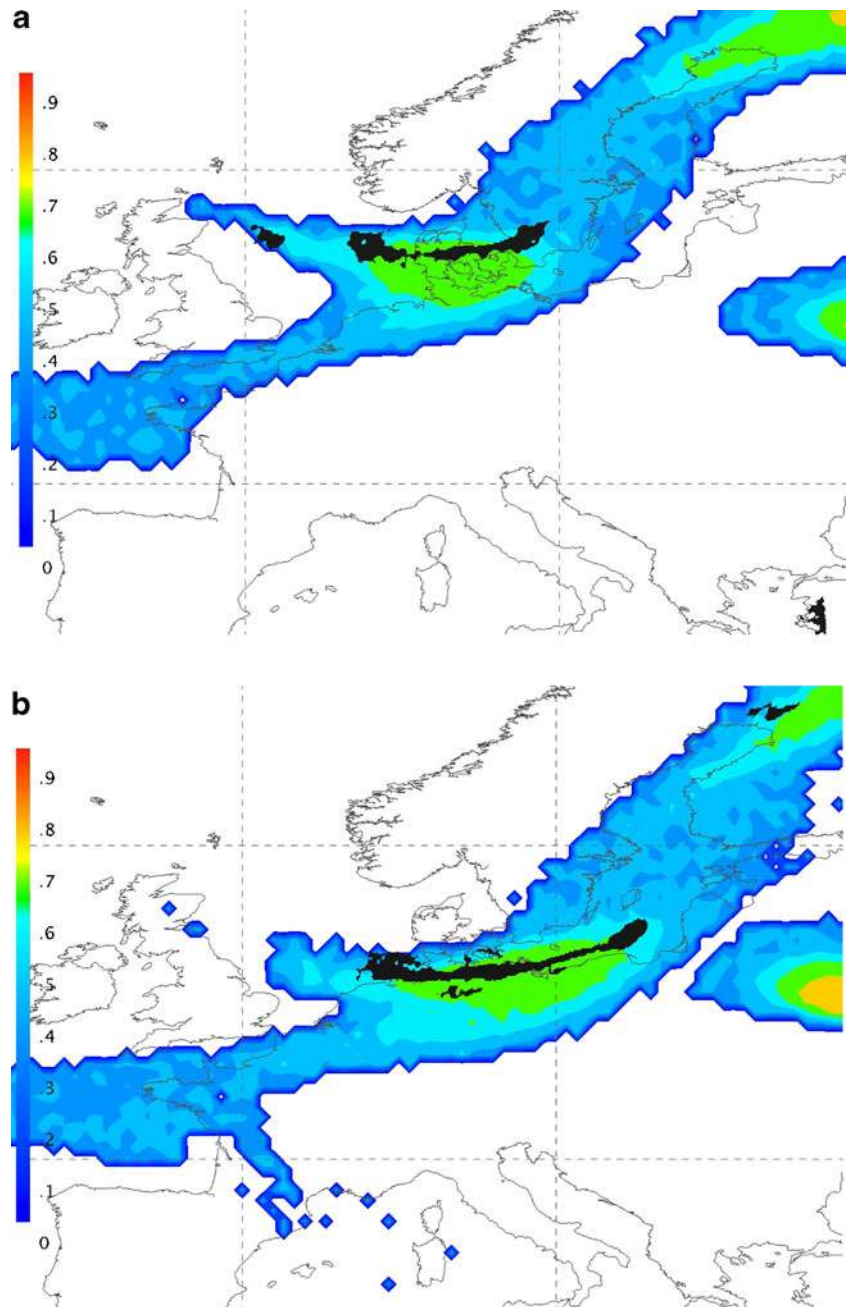
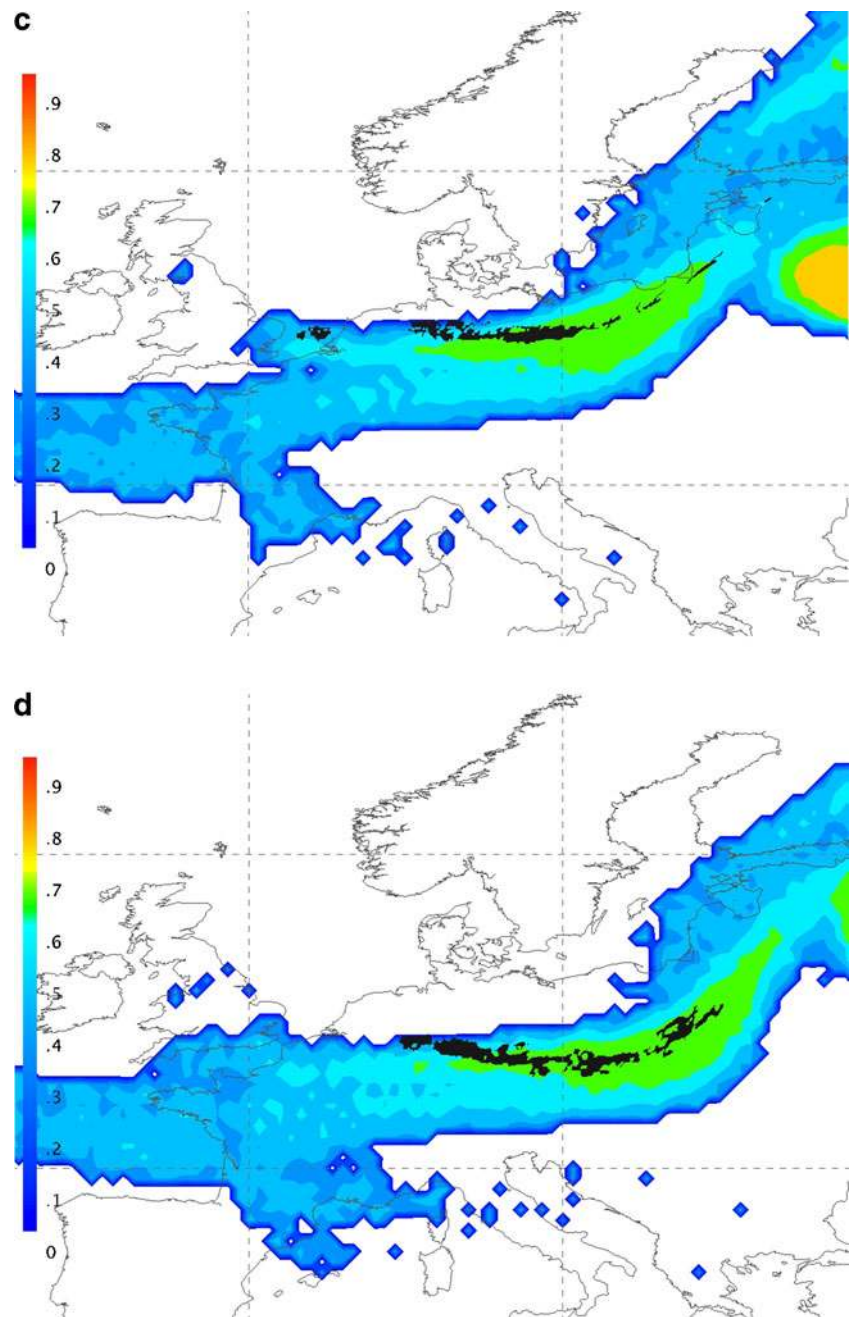


Fig. 8 (continued)



PCQWE elevation cutoff is the same as the lowest ash parcels imaged by Meteosat (124 m), the results are considerably better than those obtained using a higher cutoff (380 m—the lowest software quantization height). The number of “false positives” for the model hovers between 93 and 95 % (“Sat given PCQWE”), because the PCQWE output is nearly a superset of the Meteosat data that encompasses about 20 times the map area encompassed by the satellite data (“FMS” compared to “Sat given PCQWE”).

Thus, not only can results be output in the form of statistical moments (Figs. 5 and 7), but we have also generated outputs in the form of the probabilities directly (Fig. 8). The probability plot used herein shows the probability that ash can be

found at a given location at any altitude at the displayed time. A three-dimensional plot for a given time could also be produced, so the current two-dimensional planview is used to provide a simple demonstration of the concept. Although the current results suggest that contouring an ash cloud at about the 70 % percentile would yield a good estimate of ash position based on the comparison with the SEVIRI data, in practice, it would probably be justly conservative to choose a lower value, to reduce the possibility of encounter. Nevertheless, one important point of a probabilistic plot is that agencies and other decision-making groups can choose a statistical cut-off that they deem servicable in a given situation. The critical decision of “where to draw the line” does not



need to fall upon scientists who should primarily focus on making the best measurements and calculations possible.

A practical consideration in contemplating these results is whether they are feasible from the standpoint of computation time—can the computation be finished by the time a decision needs to be made. One run of bent takes seconds of CPU time to execute, whereas a run of puff finishes in minutes of CPU time. A sample  $9^4=6,561$  quadrature point run with  $4 \times 10^6$  puff particles was executed on 24 CPUs, each using a little less than 2 h of wall time. Given a relatively modest parallel computing capacity, therefore, the methodology executes relatively quickly.

The main conclusions from this study are the following:

1. It is possible to use other source parameters besides eruption column rise height to obtain reasonable estimates of boundary conditions important to the calculation of the loading and transport height of tephra.
2. When possible therefore, volcanologists should make and take advantage of as many measurements of source parameters as is possible.
3. Although any measurements of source parameters can be used in a model such as outlined herein, source parameter uncertainty should be addressed as vigorously as possible to minimize errors in downwind plume position and loading.
4. With respect to the source parameters for the initial, paroxysmal phase of the April 2010 Eyjafjallajökull eruption, numerical modeling with bent coupled with radiosonde data for 14 April 2010, as well as the observation that the highest model ash particles are needed to encompass the downwind ash cloud as retrieved from SEVIRI data, suggest that perhaps the initial phase of the eruption was at the high end of the parameter space explored herein, meaning that maximum MER could have been as high as  $10^8$  kg/s, and was almost certainly higher than  $10^7$  kg/s.
5. Eyjafjallajökull eruption column height was severely affected by the high winds.
6. It is critical to obtain as good as possible a picture of the weather conditions at the source, especially as given by radiosonde measurements taken close the volcano and eruption time.
7. Given the success in generating a probabilistic envelope of ash position that encompasses Meteosat-9 data (Fig. 8; Table 3), the results suggest that variations in source parameters of the type investigated here play a role in accurately estimating distal ash position.
8. PCQWE can be used to generate a probabilistic forecast of ash position for a relatively small sample size of order  $[9^4]$  computational runs.
9. The ability to generate a probabilistic forecast of ash cloud position, together with statistical moments may allow for a better separation of scientific and decision-

making tasks in eruption crises, as this frees scientists to address errors in measurement and analysis in a systematic fashion and allows decision-makers to be responsible for “drawing the line” on a region of risk.

We are currently exploring the application of PCQWE to the additional variability arising from our incomplete knowledge of the windfield. The question arises however, whether even PCQWE can provide probabilistic estimates useful in Volcanic Ash Advisories in a reasonable time. This question clearly needs to be investigated further.

**Acknowledgments** This material is based upon work supported by the National Science Foundation under grant no. EAR-1041775. The manuscript was completed under funding from AFOSR and an NSF-IDR grant. Any opinions, findings, and conclusions or recommendations expressed in this material are those of the author(s) and do not necessarily reflect the views of the National Science Foundation. Fred Prata, Armann Hoskuldsson, Thorvaldur Thordarson, and other researchers at several meetings generously discussed their own results with the authors. We thank AE M. Manga, an anonymous reviewer and C. Bonadonna for helpful, constructive criticisms of the manuscript.

## References

- Adler RJ (1981) The geometry of random fields. Wiley, London
- Augusti G, Baratta A, Casciati F (1984) Probabilistic methods in structural engineering. Chapman and Hall, London
- Ben-Haim Y, Elishakoff I (1990) Convex models of uncertainty in applied mechanics. Elsevier, Amsterdam
- Berveiller M, Sudret B, Lemaire M (2006) Stochastic finite element: a non intrusive approach by regression. *Rev Eur Mec Numer* 15:81–92
- Bonadonna C, Folch A, Loughlin S, Puempel H (2010) Ash dispersal forecast and civil aviation workshop, Geneva, Switzerland, 18–20 October 2010: Consensual document. Web document, World Meteorological Organization, Geneva, Switzerland. Available via Vhub. <http://vhub.org/resources/503>. Accessed 1 Oct 2012
- Bursik M (2001) Effect of wind on the rise height of volcanic plumes. *Geophys Res Lett* 18:3621–3624
- Bursik M, Kobs S, Burns A, Braitseva O, Bazanova L, Melekestsev I, Kurbatov A, Pieri D (2009) Volcanic plumes and the wind: jet-stream interaction examples and implications for air traffic. *J Volcanol Geotherm Res* 186:60–67
- Calder E, Sparks R, Woods A (1997) Dynamics of co-ignimbrite plumes generated from pyroclastic flows of Mount St. Helens (7 August 1980). *Bull Volcanol* 58:432–440
- Cheney EW, Kincaid D (1999) Numerical mathematics and computing. Brooks/Cole, Pacific Grove
- Chouet B, Hamiseviez N, McGetchin T (1974) Photoballistics of volcanic jet activity at Stromboli, Italy. *J Geophys Res* 79:4961–4976
- Christakos G (1992) Random field models in earth sciences. Academic, San Diego
- Clenshaw CW, Curtis AR (1960) A method for numerical integration on an automatic computer. *Numer Math* 2:197–205
- Dalbey K, Patra A, Pitman E, Bursik M, Sheridan M (2008) Input uncertainty propagation methods and hazard mapping of geophysical mass flows. *J Geophys Res* 113:B05203. doi:10.1029/2006JB004471
- Elishakoff I (1999) Whys and hows in uncertainty modelling probability, fuzziness, and anti-optimization. Springer, Berlin

- Folch A (2012) A review of tephra transport and dispersal models: evolution, current status, and future perspectives. *J Volcanol Geotherm Res* 235–236:96–115. doi:10.1016/j.jvolgeores.2012.05.020
- Folk RL, Ward WC (1957) Brazos River bar, a study in the significance of grain size parameters. *J Sediment Petrol* 27:3–27
- Glaze L, Baloga S, Wilson L (1997) Transport of atmospheric water vapour by volcanic eruption columns. *J Geophys Res* 102:6099–6108
- Graf HF, Herzog M, Oberhuber JM, Textor C (1999) Effect of environmental conditions on volcanic plume rise. *J Geophys Res* 104:24,309–24,320
- Grigoriu M (2002) Stochastic calculus applications in science and engineering. Birkhauser, Basel
- Heidinger AK, Pavolonis MJ (2009) Nearly 30 years of gazing at cirrus clouds through a split-window. Part I: methodology. *J Appl Meteorol Climatol* 48:1110–1116
- Heidinger AK, Pavolonis MJ, Holz RE, Baum BA, Berthier S (2010) Using calipso to explore the sensitivity to cirrus height in the infrared observations from npoess/viirs and goes-r/abi. *J Geophys Res* 115. doi:10.1029/2009JD012152
- Keiding JK, Sigmarrsson O (2012) Geothermobarometry of the 2010 Eyjafjallajökull eruption: new constraints on Icelandic magma plumbing systems. *J Geophys Res* 117:B00C09. doi:10.1029/2011JB008829
- LeMaitre O, Knio O, Najm H, Ghanem R (2001) A stochastic projection method for fluid flow: I. Basic formulation. *J Comput Phys* 173:481–511
- Mastin LG (2007) A user-friendly one-dimensional model for wet volcanic plumes. *Geochem Geophys Geosyst* 8:014
- Mastin L, Guffanti M, Servanckx R, Webley P, Barostti S, Dean K, Denlinger R, Durant A, Ewert J, Gardner C, Holliday A, Neri A, Rose W, Schneider D, Siebert L, Stunder B, Swanson G, Tupper A, Volentik A, Waythomas A (2009) A multidisciplinary effort to assign realistic source parameters to models of volcanic ash-cloud transport and dispersion during eruptions. *J Volcanol Geotherm Res* 186:10–21, special issue on Volcanic Ash Clouds; L. Mastin and P.W. Webley (eds.)
- Morton B, Taylor G, Turner J (1956) Gravitational turbulent convection from maintained and instantaneous sources. *Proc R Soc Lond A* 234:1–23
- Natke HG, Ben-Haim Y (1997) Uncertainty: models and measures. Akademie, Berlin
- NCEP (2009a) National Center for Environmental Prediction: Unidata online access to the operational Global Forecasting System (GFS) numerical weather prediction model. [http://motherlode.ucar.edu:8080/thredds/catalog/fmrc/NCEP/GFS/Global\\_0p5deg/catalog.html](http://motherlode.ucar.edu:8080/thredds/catalog/fmrc/NCEP/GFS/Global_0p5deg/catalog.html)
- NCEP (2009b) National Center for Environmental Prediction: Unidata online access to the operational North American Mesoscale (NAM) numerical weather prediction model. [http://motherlode.ucar.edu:8080/thredds/catalog/fmrc/NCEP/NAM/Alaska\\_11km/catalog.html](http://motherlode.ucar.edu:8080/thredds/catalog/fmrc/NCEP/NAM/Alaska_11km/catalog.html)
- Papoulis A (1984) Probability, random variables, and stochastic processes. McGraw-Hill, New York
- Pavolonis MJ (2010) Advances in extracting cloud composition information from spaceborne infrared radiances: a robust alternative to brightness temperatures. Part I: theory. *J Appl Meteorol Climatol* 49:1992–2012
- Pavolonis MJ, Feltz WF, Heidinger AK, Gallina GM (2006) A daytime complement to the reverse absorption technique for improved automated detection of volcanic ash. *J Atmos Ocean Technol* 23:1422–1444
- Petersen GN (2010) A short meteorological overview of the Eyjafjallajökull eruption 14 April–23 May 2010. *Weather* 65:203–207
- Ryall DB, Maryon RH (1998) Validation of the uk met. office name model against the etex dataset. *Atmos Environ* 32:4265–4276
- Scollo S, Prestilippo M, Coltelli M, Peterson R, Spata G (2011) A statistical approach to evaluate the tephra deposit and ash concentration from PUFF model forecasts. *J Volcanol Geotherm Res* 200:129–142
- Searcy C, Dean K, Stringer B (1998) PUFF: a high-resolution volcanic ash tracking model. *J Volcanol Geotherm Res* 80:1–16
- Shafer G (1976) A mathematical theory of evidence. Princeton University Press, Princeton
- Sparks R, Wilson L (1982) Explosive volcanic eruptions—V. Observations of plume dynamics during the 1979 Soufriere eruption, St. Vincent. *Geophys J Roy Astron Soc* 69:551–570
- Sparks RSJ, Bursik MI, Carey SN, Gilbert JS, Glaze LS, Sigurdsson H, Woods AW (1997) Volcanic plumes. Wiley, London, p 574
- Textor C, Graf H, Herzog M, Oberhuber J, Rose WI, Ernst G (2006) Volcanic particle aggregation in explosive eruption columns. Part II: numerical experiments. *J Volcanol Geotherm Res* 150:378–394
- Thorkelsson B (2012) The 2010 eruption of Eyjafjallajökull, Iceland. Tech. rep., Icelandic Meteorological Office, [http://jardvis.hi.is/sites/default/files/Pdf\\_skjol/Eyjafjallajokull\\_2010/icaoreport\\_web.pdf](http://jardvis.hi.is/sites/default/files/Pdf_skjol/Eyjafjallajokull_2010/icaoreport_web.pdf), retrieved Sept 2012
- Torquato S (2002) Random heterogeneous materials. Springer, Berlin
- Tupper A, Textor C, Herzog M, Graf HF, Richards MS (2009) Tall clouds from small eruptions: the sensitivity of eruption height and fine ash content to tropospheric instability. *Nat Hazard* 51:375–401. doi:10.1007/s11069-009-9433-9
- USN-FNMOC (2009) U.S. Navy Fleet Numerical Meteorology and Oceanography Center: Online access to the Navy Operational Global Atmospheric Prediction System numerical weather prediction model (NOGAPS). <http://www.usno.navy.mil/FNMOC/>
- Wen S, Rose WI (1994) Retrieval of sizes and total masses of particles in volcanic ash clouds using avhrr bands 4 and 5. *J Geophys Res* 99:5421–5431
- Wiener N (1938) The homogeneous chaos. *Am J Math* 60(4):897–936
- Woods AW (1993) Moist convection and the injection of volcanic ash into the atmosphere. *J Geophys Res* 98:17,627–17,636
- Woods A, Bursik M (1991) Particle fallout, thermal disequilibrium and volcanic plumes. *Bull Volcanol* 53:559–570
- WRF (2009) Online access to the Weather Research and Forecasting Model. <http://www.wrf-model.org/index.php>
- Xiu D, Hesthaven J (2005) High-order collocation methods for differential equations with random inputs. *SIAM J Sci Comput* 27:1118–1139
- Xiu D, Karniadakis GE (2002) The Wiener–Askey polynomial chaos for stochastic differential equations. *SIAM J Sci Comput* 24(2):619–644. doi:10.1137/S1064827501387826